

Dynamic correlations of frustrated quantum spins from high-temperature expansion

Ruben Burkard,¹ Benedikt Schneider,^{2,3} and Björn Sbierski¹

¹*Institut für Theoretische Physik, Universität Tübingen,
Auf der Morgenstelle 14, 72076 Tübingen, Germany*

²*Department of Physics and Arnold Sommerfeld Center for Theoretical Physics,
Ludwig-Maximilians-Universität München, Theresienstr. 37, 80333 Munich, Germany*

³*Munich Center for Quantum Science and Technology (MCQST), 80799 Munich, Germany*

(Dated: June 3, 2025)

For quantum spin systems in equilibrium, the dynamic structure factor (DSF) is among the most feature-packed experimental observables. However, from a theory perspective it is often hard to simulate in an unbiased and accurate way, especially for frustrated and high-dimensional models at intermediate temperature. We address this challenge by introducing a dynamic extension of the high-temperature expansion as an efficient numerical approach to the DSF for arbitrary lattices. We focus on the nearest-neighbor Heisenberg model and spin-lengths $S = 1/2$ and 1 . We present a user-friendly numerical implementation and provide comprehensive benchmarks on spin chains. As applications we treat a variety of frustrated two- and three dimensional antiferromagnets. In particular we shed new light on the anomalous intermediate temperature regime of the $S = 1/2$ triangular lattice model and reproduce the DSF measured recently for a $S = 1$ pyrochlore material.

Introduction.—Systems of localized quantum spins with frustrated interactions are ubiquitous in modern condensed matter experiments ranging from solid-state Mott insulators [1] to atom-based analog quantum simulators [2]. Interest arises from the hope to realize low-energy exotic correlated and topological states like quantum spin liquids (QSL) [3]. The dynamical structure factor (DSF) $S(\mathbf{k}, \omega)$ defined as spatial and temporal Fourier transform of the equilibrium two-point correlator $G_{ii'}^{\alpha\alpha'}(t) = \langle S_i^\alpha(t) S_{i'}^{\alpha'} \rangle$ is routinely measured via inelastic neutron scattering (INS) [4] in the solid-state context. For cold-atom quantum simulators the DSF is accessible via Raman spectroscopy [5]. As the DSF probes the collective spin dynamics, it contains rich information on the (dipolar) excitation spectrum, quasiparticles (or the absence thereof) and even the entanglement structure [6, 7]. From the theory perspective, however, a quantitative and unbiased calculation of the DSF for generic and possibly gapless frustrated quantum spin- S models at low temperature $T = 1/\beta$ is often challenging. With exact-diagonalization and its derivatives (e.g. finite- T Lanczos method [8]) limited to small systems and quantum Monte Carlo suffering from the sign problem, tensor networks are state-of-the-art. However, with the exception of one-dimensional (1D) systems [9], current simulations [10, 11] are only feasible for $T = 0$, small S and are still severely affected by finite-size effects and entanglement growth. Another popular bypass to spin dynamics are semiclassical approximations [12–14] which however likely miss genuine quantum effects at small S .

Here we narrow this methodological gap by introducing Dyn-HTE, a dynamic extension of the high-temperature expansion (HTE). The latter was successfully employed for more than half a century [15, 16] to compute equal-time correlations and thermodynamic observables via graph-based expansions in J/T with J the

spin-spin interaction. (Dyn-)HTE is formulated directly in the thermodynamic limit and is oblivious to frustration, entanglement, dimensionality and spin length [17] with the model-dependent available temperature range $T \gtrsim O(J/4)$ being its main limitation. On the technical level Dyn-HTE is formulated in the imaginary-time formalism but the exact frequency dependence of the expansion coefficients sets it apart from other diagrammatic approaches like pseudo-fermionic functional renormalization [18–20] or bold-line diagrammatic Monte Carlo [21]. Crucially, this enables stable analytic continuation to the real-frequency DSF while the high expansion orders ($n_{max} = 12$) typical for the conventional HTE are not compromised and go far beyond orders achievable with alternative expansion schemes for the Matsubara spin correlator [22, 23]. Further, Dyn-HTE goes considerably beyond exact-diagonalization based numerical linked-cluster expansions (NLCE) [24, 25] which have addressed the DSF for some particular $S = 1/2$ models [26], but only in the Gaussian approximation using two frequency moments of the susceptibility. In contrast, our open-source numerical implementation of Dyn-HTE [27] currently allows for $S \in \{1/2, 1\}$ Heisenberg models with a single J and typically uses four to six moments. It comes with pre-computed evaluations of generic graphs which are quickly embedded in any arbitrary user-defined lattice. Thus Dyn-HTE is a versatile, user-friendly and efficient numerical tool catering directly to experiments. We first discuss the theory background, then consider 1D benchmarks and finally applications in 2D and 3D.

Model and Matsubara correlator.—We consider length- S quantum spins S_i^α with $\alpha = x, y, z$ and ladder operators $S_i^\pm = (S_i^x \pm iS_i^y)/\sqrt{2}$ at sites \mathbf{r}_i ($i = 1, 2, \dots, N$) of an arbitrary lattice \mathcal{L} . We focus on the Heisenberg model

$$H = J \sum_{\langle ii' \rangle} (S_i^+ S_{i'}^- + S_i^- S_{i'}^+ + S_i^z S_{i'}^z), \quad (1)$$

characterized by a *single* coupling J on arbitrary bonds (ii') with $i < i'$. This includes the important case of symmetry-related nearest-neighbor interactions, but also all-to-all models or spatial disorder, e.g. vacancies. We assume the absence of magnetic fields. None of these assumptions or the spin-rotation symmetries of (1) are essential for Dyn-HTE and can be relaxed in future developments analogous to conventional HTE [16, 17, 28, 29].

We approach the spin correlator in the imaginary-time formalism [30] which treats thermal density matrix and operator evolution $S_i^z(\tau) = e^{H\tau} S_i^z e^{-H\tau}$ on equal footing. The Matsubara correlator at frequency $\nu_m = 2\pi Tm$ ($m \in \mathbb{Z}$) and its HTE to order n_{max} in $x = J/T$ read

$$\begin{aligned} TG_{ii'}(i\nu_m) &= T^2 \int_0^\beta d\tau d\tau' e^{i\nu_m(\tau-\tau')} \langle \mathcal{T} S_i^z(\tau) S_{i'}^z(\tau') \rangle (2) \\ &= p_{ii'}^{(0)}(x) \delta_{0,m} + \sum_{r=1}^{n_{max}} p_{ii'}^{(2r)}(x) x^{2r} \Delta_{2\pi m}^{2r} + O(x^{n_{max}+1}) (3) \end{aligned}$$

Here \mathcal{T} enforces τ -ordering, $\Delta_y \equiv (1 - \delta_{0,y})/y$ and $r_{max} = \lfloor n_{max}/2 \rfloor$. The polynomials $p_{ii'}^{(2r)}(x)$ are of degree $n_{max} - 2r$ with rational coefficients and are provided by our open-source numerical implementation [27] for all site-pairs ii' on *arbitrary* lattices \mathcal{L} . This flexibility hinges on the pre-evaluation of the Dyn-HTE (3) for abstract graphs which can then be embedded in any \mathcal{L} like in conventional HTE [16]. The efficient evaluation of *all* $\simeq 1.6 \times 10^6$ graphs with up to $n_{max} = 12$ edges ($\sim J$) [currently for $S \in \{\frac{1}{2}, 1\}$] rests on a recursive formulation of perturbation theory and the exact solution of the up to $n_{max} + 2$ -fold τ -integrals using the kernel trick [31], see our technical companion article Ref. 32 for details. There we also discuss results and applications for the *static* spin susceptibility encoded in the zero-frequency Matsubara correlator $G_{ii'}(i\nu_m = 0)$.

DSF and stable analytical continuation.—The real-frequency DSF for translation invariant \mathcal{L} is defined as

$$S(\mathbf{k}, \omega) = \int_{-\infty}^{+\infty} \frac{dt}{2\pi N} \sum_{i,i'} e^{i\omega t - i\mathbf{k} \cdot (\mathbf{r}_i - \mathbf{r}_{i'})} \langle S_i^z(t) S_{i'}^z \rangle (4)$$

and relates to the imaginary part of the dynamical susceptibility via the fluctuation-dissipation relation [30], $A_{\mathbf{k}}(\omega) = 2\pi(1 - e^{-\omega\beta})S(\mathbf{k}, \omega)$. From the Lehmann representation, the exact $A_{\mathbf{k}}(\omega)$ fulfills $A_{\mathbf{k}}(\omega > 0) \geq 0$ and $A_{\mathbf{k}}(\omega) = -A_{-\mathbf{k}}(-\omega)$. It relates to the momentum-space version of the Matsubara correlator (2) as

$$G_{\mathbf{k}}(i\nu_m) = \frac{1}{2\pi} \int_{-\infty}^{\infty} d\omega \frac{A_{\mathbf{k}}(\omega)}{\omega - i\nu_m}. (5)$$

This is strictly correct only for $m \neq 0$ and an additional term quantifying long-term memory effects and non-ergodicity appears on the right-hand side for $m = 0$ [33–35]. For systems of interest in this work we assume such effects are absent and thus continue with Eq. (5).

For numerical methods that provide noisy data for $G_{\mathbf{k}}(i\nu_m)$ limited to a finite frequency range the inversion of Eq. (5) is notoriously unstable. In contrast, the explicit frequency dependence provided by Dyn-HTE in Eq. (3) allows for a stable analytical continuation algorithm producing a *faithful* (non-negative and properly symmetric) $A_{\mathbf{k}}(\omega)$ [36–40]. Here we assume inversion symmetry such that $A_{\mathbf{k}}(\omega) = A_{-\mathbf{k}}(\omega)$ is antisymmetric in ω and $G_{\mathbf{k}}(i\nu_m)$ is real [32]. For inversion-breaking systems the following can be straightforwardly generalized using the symmetric and anti-symmetric combination $A_{\mathbf{k}}^\pm(\omega) \equiv \frac{1}{2} [A_{\mathbf{k}}(\omega) \mp A_{-\mathbf{k}}(-\omega)]$ which fulfill the analog of Eq. (5) with the imaginary and real part of $G_{\mathbf{k}}(i\nu_m)$ on the left-hand side, respectively.

As a first step, we define $w = \omega/J$ and expand the right-hand side of Eq. (5) in (even) powers of $1/\nu_m$,

$$TG_{\mathbf{k}}(i\nu_m) = \int_{-\infty}^{\infty} dw R_{\mathbf{k}}(w) \left[\delta_{m,0} - \sum_{r=1,2,\dots} (iwx\Delta_{2\pi m})^{2r} \right], (6)$$

with $R_{\mathbf{k}}(w) \equiv TA_{\mathbf{k}}(\omega)/(2\pi w)$ the relaxation function [38]. Comparing Eq. (6) to the HTE of Eq. (3) we identify the spatial Fourier transform of the polynomials $p_{ii'}^{(2r)}(x)$ with the HTE of the relaxation function's (even) frequency moments [for $r > 0$, there is a relative sign $-(-1)^r$],

$$m_{\mathbf{k},2r} = \int_{-\infty}^{\infty} dw w^{2r} R_{\mathbf{k}}(w), \quad r = 0, 1, 2, \dots (7)$$

To discuss the reconstruction of a faithful relaxation function [and hence $A_{\mathbf{k}}(\omega)$] from the HTE of its moments, we first pretend the latter are known exactly for all $r = 0, 1, 2, \dots$ and drop the label \mathbf{k} for brevity. We

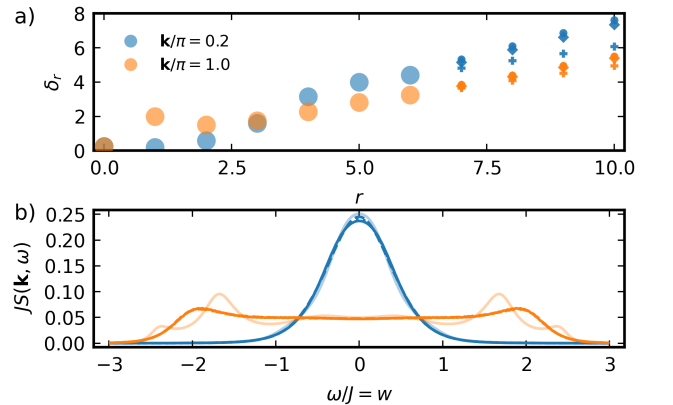


FIG. 1. Heisenberg $S = 1/2$ AFM chain at $T = \infty$. (a) Continued fraction parameters δ_r for two momenta \mathbf{k} . The large dots denote the exact results for $r = 0, 1, \dots, 6$ from Dyn-HTE, the small markers depict various linear extrapolation schemes $\delta_{r>6} = ra + b$ with $b = 0$ or $b \neq 0$. (b) DSF obtained from the n -pole truncation (10). Transparent lines use only the exactly known δ_r for $r \leq 6$, remaining lines employ the linear extrapolation schemes to $r'_{max} = 2000$. We use $\eta = O(0.01)$ small enough so that the results do not depend on it.

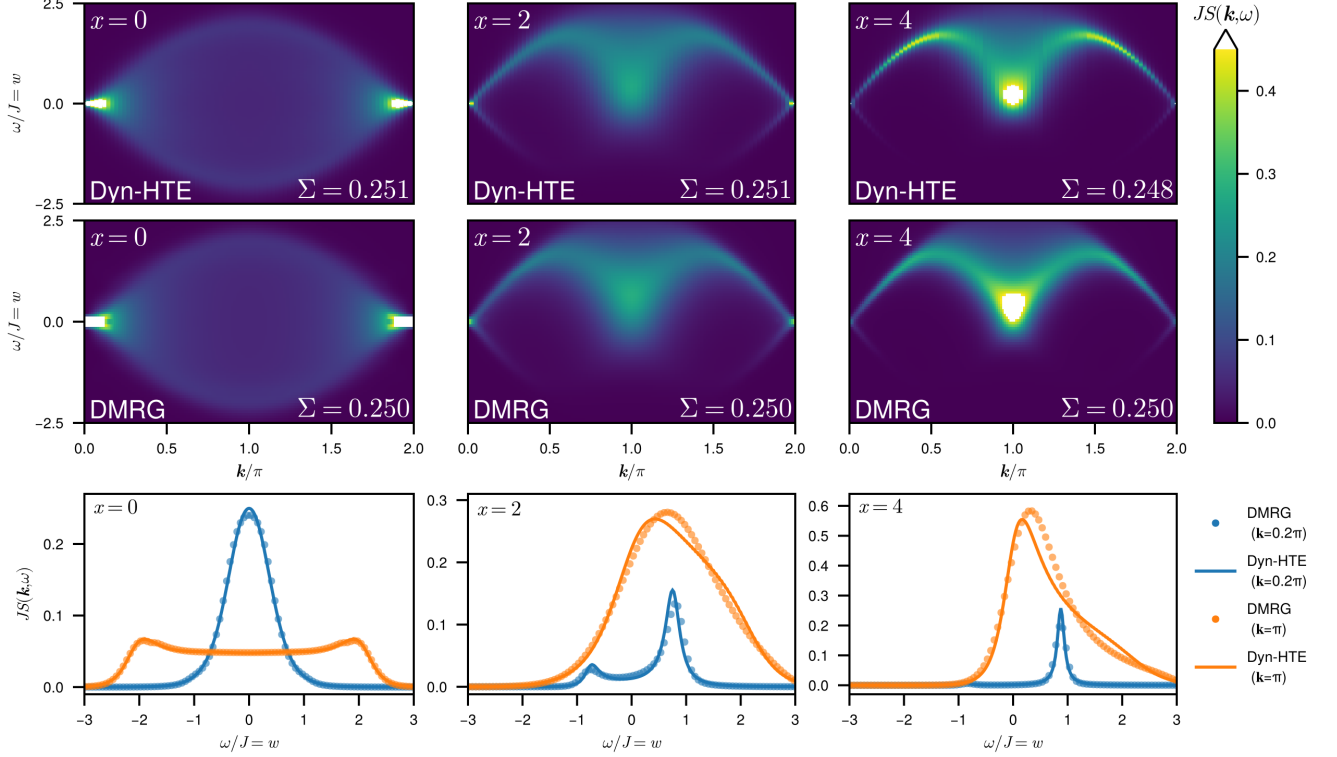


FIG. 2. DSF for the Heisenberg $S = 1/2$ AFM chain at $x = J/T \in \{0, 2, 4\}$, left to right column. Top row: Dyn-HTE results based on resummation of moments with $r \leq 6$ ($r \leq 3$ for $x > 0$). Middle row: DMRG data reproduced from Ref. 9. Bottom row: Lineshape for $S(\mathbf{k}, \omega)$ at fixed $\mathbf{k} \in \{0.2\pi, \pi\}$. The lattice spacing is set to unity. The values for $\Sigma \equiv \frac{J}{V_{BZ}} \int_{-\infty}^{\infty} d\omega \int_{BZ} d\mathbf{k} S(\mathbf{k}, \omega)$ with V_{BZ} the BZ-volume are also indicated and Dyn-HTE fulfills the sum-rule $\Sigma = \langle S_i^z S_i^z \rangle = S(S+1)/3 = 1/4$ within $< 1\%$.

consider the Laplace transform of the relaxation function with complex argument [36, 37] $\tilde{R}(s) = \int_{-\infty}^{\infty} dv \frac{R(v)}{s - iv}$ which we represent as a continued fraction with $\delta_r \geq 0$,

$$\tilde{R}(s) = \frac{\delta_0}{s+} \frac{\delta_1}{s+} \frac{\delta_2}{s+} \frac{\delta_3}{s+} \dots \quad (8)$$

Matching the $1/s$ -expansions of both expressions we determine δ_r from the moments m_0, m_2, \dots, m_{2r} . For example, we have $\delta_0 = m_0$, $\delta_1 = m_2/m_0$, $\delta_2 = m_4/m_2 - m_2/m_0$ and $\delta_3 = m_0(m_4^2 - m_2m_6)/[m_2^3 - m_0m_2m_4]$. For the remaining $\delta_{4,5,6}$ required for $r_{max} = 6$, see End Matter. Reinstating \mathbf{k} , the (faithful) $A_{\mathbf{k}}(\omega)$ is

$$JA_{\mathbf{k}}(\omega) = 2xw \operatorname{Re}[\tilde{R}_{\mathbf{k}}(s = iw + \eta)]. \quad (9)$$

with η a positive infinitesimal and the DSF follows from the fluctuation-dissipation relation below Eq. (4).

Heisenberg $S = 1/2$ AFM chain.—To discuss how to adapt this idealized analytical continuation procedure for the Dyn-HTE data of Eq. (3) we turn to the well-studied nearest-neighbor Heisenberg $S = 1/2$ anti-ferromagnet (AFM) in 1D for benchmark. Due to finite expansion order $n_{max} = 12$, the HTE is only available for a finite number of moments $m_{\mathbf{k}, 2r}$ with $r = 0, 1, \dots, r_{max}$ with

$r_{max} = 6$. To show how to deal with this restriction, we first consider the infinite- T case ($x = 0$) so that the moments are exactly given by the x^0 -coefficients of their HTEs. We convert to the δ_r and plot them in Fig. 1(a) for two representative momenta $\mathbf{k} = 0.2\pi$ and π (large dots). To avoid sharp Dirac-Delta peaks in $A_{\mathbf{k}}(\omega)$ resulting from a straightforward truncation of Eq. (8) we first invoke broadening via the n -pole truncation [38]

$$\tilde{R}_{r_{max}}(s) = \frac{\delta_0}{s+} \frac{\delta_1}{s+} \frac{\delta_2}{s+} \dots \frac{\delta_{r_{max}-2}}{s+} \frac{\delta_{r_{max}-1}}{s + \sqrt{\delta_{r_{max}}}}, \quad (10)$$

with the resulting DSF shown as a transparent line in Fig. 1(b). Following Ref. 37 we improve on this approximation by linear extrapolation of δ_r to $r'_{max} = O(1000)$ and only then apply truncation (10) with $r_{max} \rightarrow r'_{max}$. The different small markers in Fig. 1(a) correspond to various linear extrapolation schemes (c.f. figure caption) to which the resulting DSF shown in various opaque linestyles in Fig. 1(b) is practically insensitive. The so obtained DSF is in excellent agreement with DMRG [9] throughout the Brillouin zone (BZ), see Fig. 2, left column. Note however that for moments at $T = \infty$ the recursion method [37, 41] is more efficient than Dyn-HTE tailored to finite $T < \infty$ (which means $x > 0$).

For $x > 0$, recall that Dyn-HTE only provides the expansion of the moments $m_{\mathbf{k},2r}(x)$ to order $n_{max} - 2r$ in x . Hence, for the interesting regime $x \gtrsim 1$ beyond convergence of the bare series, we apply resummation in form of Padé approximants [16] to $m_{\mathbf{k},2r}(x)$ with $r \leq 3$ and then proceed as above, see End Matter (Fig. 5) for details. Analogous to conventional HTE [16, 42] we improve convergence by changing to the auxiliary variable $u = \tanh(fx)$ with tuning parameter f chosen such that different Padé approximants agree. In principle, f should be as small as possible to reach large x and could vary with \mathbf{k} but for the chain a single $f = 0.48$ works well. The 2nd and 3rd column of Fig. 2 compare the DSF at temperatures $x = 2$ and 4 from Dyn-HTE (top) to DMRG [9] (middle). Linecuts (bottom) show only minor deviations.

$S = 1/2$ Heisenberg AFMs in 2D.—While magnetic long-range order is only possible at $T = 0$ for these nearest-neighbor models, its precursor in the form of spin-waves can dominate the DSF already at temperatures $T \lesssim J$ [43]. We refer to the End Matter for representative Dyn-HTE results for the DSF of the square lattice model. There, we also consider the frustrated kagome-lattice which lacks long-range magnetic order at $T = 0$ and shows broad features in the DSF.

Here we focus on the triangular lattice model with 120° -order at $T = 0$ [44]. For $\frac{1}{4} \lesssim T/J \lesssim 1$, however, an enigmatic anomaly occurs: As first seen from HTE, static properties deviate strongly from renormalized-classical spin-wave predictions [45–47]. For example, at $T = J/4$, the correlation length is relatively small (about a lattice constant) and the entropy per spin is large ($\simeq \ln 2/3$).

The DSF from Dyn-HTE shown in Fig. 3 (see also End Matter for a BZ-path at $x = 3$) is ideally suited to shed new light on the still debated nature of this intermediate- T regime. One proposed scenario starts from the $T = 0$ excitation spectrum which shows a “roton-like excitation” (RLE) characterized by a dispersion minimum at the M -point (center of BZ edge) with gap $\Delta \simeq 0.55J$ [48, 49]. Is the intermediate- T region primarily characterized by thermal excitations of these enigmatic RLEs? At $\mathbf{k} = M$, the T -dependence of the equal-time structure factor shows a weak maximum around $T \simeq \Delta$ [47] but the DSF from Dyn-HTE in Fig. 3(top) does not soften significantly across the intermediate T -range with the peak remaining around $\omega_{max} \simeq J$ [for $S(\mathbf{k} = M, \omega \rightarrow 0)$, a weak maximum can however be found as T decreases]. Hence, if the RLE at $\mathbf{k} = M$ is responsible for the anomalous behavior, the associated fluctuations are not simple spin-waves but must be more complex. One candidate are triangle-based chiral fluctuations [47] but the associated DSF via Dyn-HTE is beyond scope of this work.

An alternative scenario links the anomalous intermediate- T regime to the passage through a critical fan [50] of a $T = 0$ quantum phase transition (QPT) at which the 120° order melts [46, 51, 52]. The QPT appears in an extended model parameter

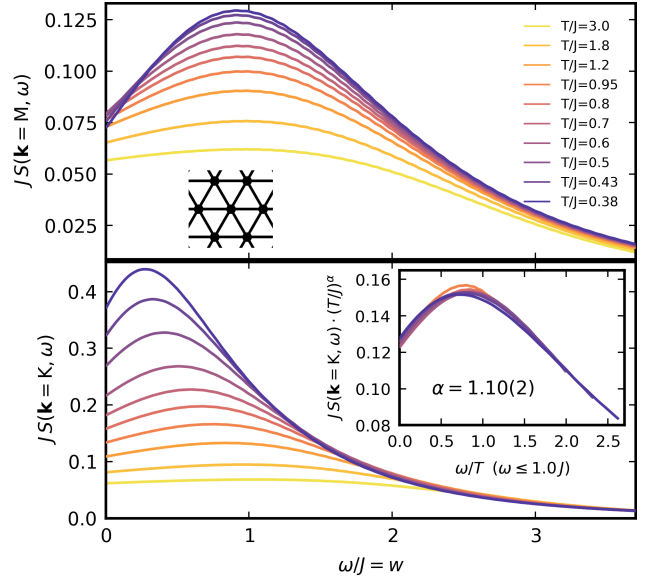


FIG. 3. DSF of triangular lattice $S = 1/2$ Heisenberg AFM at momenta M (top) and K (bottom) from Dyn-HTE with $r_{max} = 3$ and $f = 0.55$. Inset: ω/T -scaling collapse for $\omega \leq J$ and $0.43 \leq T/J \leq 0.95$ with scaling exponent $\alpha = 1.10(2)$.

space, one candidate is the J_1 - J_2 -model with a QSL at $J_2 \gtrsim 0.06J_1$ [53]. A hallmark of the critical-fan scenario is a temperature-frequency scaling relation for the DSF at ordering wavevector $\mathbf{k} = K$ [51] for $|\omega| \lesssim J$,

$$JS(\mathbf{k} = K, \omega)(T/J)^\alpha = \Phi(\omega/T), \quad (11)$$

where $\alpha = (2-\eta)/z$ is determined by the (unknown) critical exponents of the QPT and $\Phi(\cdot)$ is a scaling function. Interestingly, the $\mathbf{k} = K$ DSF from Dyn-HTE shown in Fig. 3(bottom) fulfills such a relation for $\alpha = 1.10(2)$ (inset), but the T -range for which scaling occurs is relatively narrow. If scaling holds indeed and the lower limit on T is not due to inaccuracies of Dyn-HTE, extensions to the J_1 - J_2 -model should be able to tune closer to criticality and thereby widen the T -range used for scaling. Other open questions pertain to the incompatible value of $\alpha \simeq 1.73(12)$ found from a similar scaling analysis of INS data from KYbSe_2 with finite and slightly subcritical J_2 [54] and an extended scaling analysis taking into account deviations from the ordering wavevector, $\mathbf{k} \neq K$.

$S = 1$ Heisenberg AFMs: Chain and pyrochlore lattice.—Finally we obtain the DSF from Dyn-HTE for spin $S = 1$ Heisenberg AFMs. For the chain at $x = 4$, some aspects like the dispersion maxima or Haldane gap already agree well with ground-state tensor-network results, see End Matter (Fig. 7). The $S = 1$ pyrochlore material $\text{NaCaNi}_2\text{F}_7$ was reported to approximately realize the nearest-neighbor Heisenberg AFM [12, 55] but also possible biquadratic interactions were discussed [56]. We assume $J = 2.4 \text{ meV}$ [56] and compare the DSF from Dyn-

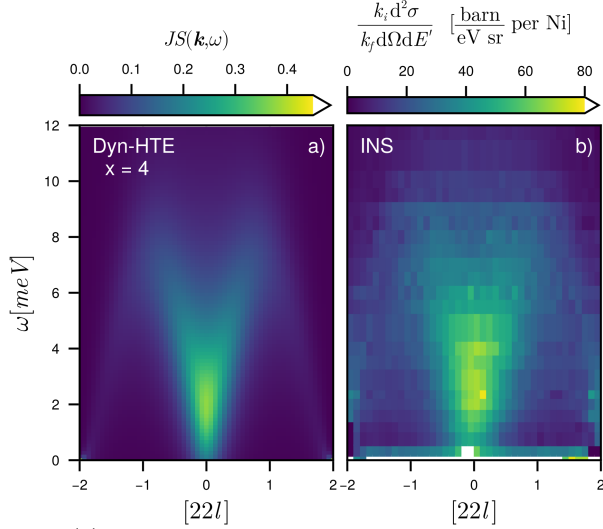


FIG. 4. (a) DSF for the pyrochlore lattice $S = 1$ Heisenberg AFM for $\mathbf{k} = (2, 2, l)$, $J = 2.4 \text{ meV}$ at $x = J/T = 4$ from Dyn-HTE (via u-Padé with $f = 0.6$). (b) Corresponding experimental INS data for $\text{NaCaNi}_2\text{F}_7$ at $x \simeq 15$ (from Ref. [55]).

HTE along the $[22l]$ slice with the experimental INS result [55], see Fig. 4. We find good agreement of the main features including the size of the “V” shape as well as the dome of spectral weight at high ω . In Dyn-HTE, the maximum along the line-cut at $[220]$ appears at slightly lower ω compared to the INS data. A possible reason is the mismatch in temperature ($x = 4$ in Dyn-HTE versus $x \simeq 15$ in INS), indeed the peak position in Dyn-HTE has a trend to higher ω with lower T .

Conclusion.—Compared to static observables from conventional HTE, the DSF obtained via Dyn-HTE accesses a wealth of additional information on dipolar excitations. Depending on the model, the results can be trusted up to $x = J/T \simeq 4$ but application of advanced resummation strategies [57] might extend this range.

Looking ahead, Dyn-HTE will not only be useful to understand INS data but also informs experiments with local probes like muon spin relaxation [4], inelastic electron tunneling spectroscopy for 2D quantum magnets [58, 59] or noise spectroscopy [60]. Other applications include finite- T spin diffusion and the computation of quantum Fisher information as entanglement witness [6, 9]. Straightforward extensions of the Dyn-HTE formalism will consider $S > 1$, models with more than one coupling constant (e.g. J_1 - J_2) [61], single-ion anisotropies or magnetic fields [29]. Another worthwhile endeavor would be the extension to higher-order dynamic [62, 63] or chiral [22, 47, 64] correlators which are recently moving into focus.

Acknowledgments.—We thank Michel Ferrero, Wei Li, Matías Gonzalez, Alexander Tsirlin, Johannes Reuther, Kemp Plumb and Andreas Weichselbaum for useful discussions and the latter two for sharing tensor network data from Ref. 9 and INS data from Ref. 55, respectively. The authors acknowledge the Gauss Centre for

Supercomputing e.V. (www.gauss-centre.eu) for funding this project by providing computing time through the John von Neumann Institute for Computing (NIC) on the GCS Supercomputer JUWELS at Jülich Supercomputing Centre (JSC). The authors also acknowledge support by the state of Baden-Württemberg through bwHPC and the German Research Foundation (DFG) through Grant No. INST 40/575-1 FUGG (JUSTUS 2 cluster). We acknowledge funding from the Deutsche Forschungsgemeinschaft (DFG, German Research Foundation) through the Research Unit FOR 5413/1, Grant No. 465199066. B.Sch. acknowledges funding from the Munich Quantum Valley, supported by the Bavarian state government with funds from the Hightech Agenda Bayern Plus. B.Sb. and B.Sch. are supported by DFG Grant No. 524270816.

-
- [1] C. Broholm, R. J. Cava, S. A. Kivelson, D. G. Nocera, M. R. Norman, and T. Senthil, Quantum spin liquids, *Science* **367**, eaay0668 (2020).
 - [2] A. Browaeys and T. Lahaye, Many-Body Physics with Individually-Controlled Rydberg Atoms, *Nature Physics* **16**, 132 (2020).
 - [3] L. Savary and L. Balents, Quantum spin liquids: A review, *Reports on Progress in Physics* **80**, 016502 (2016).
 - [4] J. Khatua, B. Sana, A. Zorko, M. Gomilšek, K. S. M. S. R. Rao, M. Baenitz, B. Schmidt, and P. Khuntia, Experimental signatures of quantum and topological states in frustrated magnetism, *Physics Reports* **1041**, 1 (2023).
 - [5] M. L. Prichard, Z. Ba, I. Morera, B. M. Spar, D. A. Huse, E. Demler, and W. S. Bakr, *Observation of Magnon-Polarons in the Fermi-Hubbard Model* (2025), arXiv:2502.06757.
 - [6] P. Hauke, M. Heyl, L. Tagliacozzo, and P. Zoller, Measuring multipartite entanglement through dynamic susceptibilities, *Nature Physics* **12**, 778 (2016).
 - [7] P. Laurell, A. Scheie, E. Dagotto, and D. A. Tennant, Witnessing Entanglement and Quantum Correlations in Condensed Matter: A Review, *Advanced Quantum Technologies* **8**, 2400196 (2025).
 - [8] P. Prelovšek, M. Gomilšek, T. Arh, and A. Zorko, Dynamical spin correlations of the kagome antiferromagnet, *Physical Review B* **103**, 014431 (2021).
 - [9] L. L. Kish, A. Weichselbaum, D. M. Pajerowski, A. T. Savici, A. Podlesnyak, L. Vasylechko, A. Tsvelik, R. Konik, and I. A. Zaliznyak, *High-temperature quantum coherence of spinons in a rare-earth spin chain* (2024), arXiv:2406.16753.
 - [10] M. Drescher, L. Vanderstraeten, R. Moessner, and F. Pollmann, Dynamical signatures of symmetry-broken and liquid phases in an $S = 1/2$ Heisenberg antiferromagnet on the triangular lattice, *Physical Review B* **108**, L220401 (2023).
 - [11] N. E. Sherman, M. Dupont, and J. E. Moore, Spectral function of the J_1 - J_2 Heisenberg model on the triangular lattice, *Physical Review B* **107**, 165146 (2023).
 - [12] S. Zhang, H. J. Changlani, K. W. Plumb, O. Tchernyshyov, and R. Moessner, Dynamical structure factor of the three-dimensional quantum spin liquid candi-

- date NaCaNi₂F₇, *Physical Review Letters* **122**, 167203 (2019).
- [13] D. Dahlbom, H. Zhang, C. Miles, S. Quinn, A. Niraula, B. Thipe, M. Wilson, S. Matin, H. Mankad, S. Hahn, D. Pajerowski, S. Johnston, Z. Wang, H. Lane, Y. W. Li, X. Bai, M. Mourigal, C. D. Batista, and K. Barros, *Sunny.jl: A Julia Package for Spin Dynamics* (2025), arXiv:2501.13095 [quant-ph].
 - [14] C. Kim and M. Mourigal, *Emulation of quantum correlations by classical dynamics in a spin-1/2 Heisenberg chain* (2025), arXiv:2503.19975 [cond-mat].
 - [15] C. Domb and M. S. Green, *Phase Transitions and Critical Phenomena / Vol. 3, Series Expansions for Lattice Models*, Phase Transitions and Critical Phenomena (Academic Press, London, 1974).
 - [16] J. Oitmaa, C. Hamer, and W. Zheng, *Series Expansion Methods for Strongly Interacting Lattice Models* (Cambridge University Press, Cambridge, 2006).
 - [17] A. Lohmann, H.-J. Schmidt, and J. Richter, Tenth-order high-temperature expansion for the susceptibility and the specific heat of spin-s Heisenberg models with arbitrary exchange patterns: Application to pyrochlore and kagome magnets, *Physical Review B* **89**, 014415 (2014).
 - [18] J. Reuther and P. Wölfle, J1-J2 frustrated two-dimensional Heisenberg model: Random phase approximation and functional renormalization group, *Physical Review B* **81**, 144410 (2010).
 - [19] N. Niggemann, B. Sbierski, and J. Reuther, Frustrated quantum spins at finite temperature: Pseudo-Majorana functional renormalization group approach, *Physical Review B* **103**, 104431 (2021).
 - [20] T. Müller, D. Kiese, N. Niggemann, B. Sbierski, J. Reuther, S. Trebst, R. Thomale, and Y. Iqbal, Pseudofermion functional renormalization group for spin models, *Reports on Progress in Physics* **87**, 036501 (2024).
 - [21] S. A. Kulagin, N. Prokof'ev, O. A. Starykh, B. Svistunov, and C. N. Varney, Bold diagrammatic Monte Carlo technique for frustrated spin systems, *Physical Review B* **87**, 024407 (2013).
 - [22] A. Rückriegel, D. Tarasevych, J. Krieg, and P. Kopietz, Recursive algorithm for generating high-temperature expansions for spin systems and the chiral nonlinear susceptibility, *Physical Review B* **110**, 144416 (2024).
 - [23] B. Schneider, R. Burkard, B. Olmos, I. Lesanovsky, and B. Sbierski, Dipolar ordering transitions in many-body quantum optics: Analytical diagrammatic approach to equilibrium quantum spins, *Physical Review A* **110**, 063301 (2024).
 - [24] M. Rigol, T. Bryant, and R. R. P. Singh, Numerical linked-cluster algorithms. I. Spin systems on square, triangular, and kagomé lattices, *Physical Review E* **75**, 061118 (2007).
 - [25] B. Tang, E. Khatami, and M. Rigol, A short introduction to numerical linked-cluster expansions, *Computer Physics Communications* **184**, 557 (2013).
 - [26] N. E. Sherman and R. R. P. Singh, Structure factors of the kagome-lattice Heisenberg antiferromagnets at finite temperatures, *Physical Review B* **97**, 014423 (2018).
 - [27] bsbierski/Dyn-HTE: Dynamic correlations of quantum spins from high-temperature expansion (2025).
 - [28] H. Rosner, R. R. P. Singh, W. H. Zheng, J. Oitmaa, and W. E. Pickett, High-temperature expansions for the J1 - J2 Heisenberg models: Applications to *ab initio* calculated models for Li₂VOSiO₄ and Li₂VOGeO₄, *Physical Review B* **67**, 014416 (2003).
 - [29] L. Pierre, B. Bernu, and L. Messio, High temperature series expansions of $S = 1/2$ Heisenberg spin models: algorithm to include the magnetic field with optimized complexity, *SciPost Physics* **17**, 105 (2024).
 - [30] H. Bruus, K. Flensberg, H. Bruus, and K. Flensberg, *Many-Body Quantum Theory in Condensed Matter Physics: An Introduction*, Oxford Graduate Texts (Oxford University Press, Oxford, New York, 2004).
 - [31] J. Halbinger, B. Schneider, and B. Sbierski, Spectral representation of Matsubara n-point functions: Exact kernel functions and applications, *SciPost Physics* **15**, 183 (2023).
 - [32] R. Burkard, B. Schneider, and B. Sbierski, *Dyn-HTE: High-temperature expansion of the dynamic Matsubara spin correlator* (2025), arXiv:2505.14571.
 - [33] P. C. Kwok and T. D. Schultz, Correlation functions and Green functions: zero-frequency anomalies, *Journal of Physics C: Solid State Physics* **2**, 1196 (1969).
 - [34] M. Suzuki, Ergodicity, constants of motion, and bounds for susceptibilities, *Physica* **51**, 277 (1971).
 - [35] C. Watzenböck, M. Feller, K. Held, and A. Toschi, Long-term memory magnetic correlations in the Hubbard model: A dynamical mean-field theory analysis, *SciPost Physics* **12**, 184 (2022).
 - [36] H. Mori, A Continued-Fraction Representation of the Time-Correlation Functions, *Progress of Theoretical Physics* **34**, 399 (1965).
 - [37] V. S. Viswanath and Müller, Gerhard, *The Recursion Method: Application to Many-Body Dynamics*, Lecture Notes in Physics Monographs No. v.23 (Springer Berlin / Heidelberg, 1994).
 - [38] S. W. Lovesey and R. A. Meserve, Dynamic properties of a one-dimensional Heisenberg magnet, *Physical Review Letters* **28**, 614 (1972).
 - [39] S. Pairault, D. Senechal, and A.-M. S. Tremblay, Strong-Coupling Perturbation Theory of the Hubbard Model, *The European Physical Journal B* **16**, 85 (2000).
 - [40] E. Perepelitsky, A. Galatas, J. Mravlje, R. Žitko, E. Khatami, B. S. Shastry, and A. Georges, Transport and optical conductivity in the Hubbard model: A high-temperature expansion perspective, *Physical Review B* **94**, 235115 (2016).
 - [41] P. Jung, R. W. Helmes, and A. Rosch, Transport in Almost Integrable Models: Perturbed Heisenberg Chains, *Physical Review Letters* **96**, 067202 (2006).
 - [42] N. Elstner and A. P. Young, Spin-1/2 Heisenberg antiferromagnet on the kagome lattice: High-temperature expansion and exact-diagonalization studies, *Physical Review B* **50**, 6871 (1994).
 - [43] S. Chakravarty, B. I. Halperin, and D. R. Nelson, Two-dimensional quantum Heisenberg antiferromagnet at low temperatures, *Physical Review B* **39**, 2344 (1989).
 - [44] L. Capriotti, A. E. Trumper, and S. Sorella, Long-Range Néel Order in the Triangular Heisenberg Model, *Physical Review Letters* **82**, 3899 (1999).
 - [45] N. Elstner, R. R. P. Singh, and A. P. Young, Finite temperature properties of the spin-1/2 Heisenberg antiferromagnet on the triangular lattice, *Physical Review Letters* **71**, 1629 (1993).
 - [46] E. A. Ghioldi, M. G. Gonzalez, S.-S. Zhang, Y. Kamiya, L. O. Manuel, A. E. Trumper, and C. D. Batista, Dynamical structure factor of the triangular antiferromagnet: Schwinger boson theory beyond mean field, *Physical Review B* **67**, 014416 (2003).

- Review B **98**, 184403 (2018).
- [47] L. Chen, D.-W. Qu, H. Li, B.-B. Chen, S.-S. Gong, J. v. Delft, A. Weichselbaum, and W. Li, Two-temperature scales in the triangular-lattice Heisenberg antiferromagnet, *Physical Review B* **99**, 140404 (2019).
 - [48] W. Zheng, J. O. Fjærestad, R. R. P. Singh, R. H. McKenzie, and R. Coldea, Anomalous Excitation Spectra of Frustrated Quantum Antiferromagnets, *Physical Review Letters* **96**, 057201 (2006).
 - [49] O. A. Starykh, A. V. Chubukov, and A. G. Abanov, Flat spin-wave dispersion in a triangular antiferromagnet, *Physical Review B* **74**, 180403 (2006).
 - [50] S. Sachdev, *Quantum Phase Transitions*, 2nd ed. (Cambridge University Press, Cambridge, 2011).
 - [51] S. Sachdev and J. Ye, Universal quantum-critical dynamics of two-dimensional antiferromagnets, *Physical Review Letters* **69**, 2411 (1992).
 - [52] A. V. Chubukov, S. Sachdev, and T. Senthil, Quantum phase transitions in frustrated quantum antiferromagnets, *Nuclear Physics B* **426**, 601 (1994).
 - [53] Z. Zhu and S. R. White, Spin liquid phase of the $S = 1/2$ J1-J2 Heisenberg model on the triangular lattice, *Physical Review B* **92**, 041105 (2015).
 - [54] A. O. Scheie, E. A. Ghioldi, J. Xing, J. A. M. Paddison, N. E. Sherman, M. Dupont, L. D. Sanjeewa, S. Lee, A. J. Woods, D. Abernathy, D. M. Pajerowski, T. J. Williams, S.-S. Zhang, L. O. Manuel, A. E. Trumper, C. D. Pemmaraju, A. S. Sefat, D. S. Parker, T. P. Devereaux, R. Movshovich, J. E. Moore, C. D. Batista, and D. A. Tennant, Proximate spin liquid and fractionalization in the triangular antiferromagnet KYbSe₂, *Nature Physics* **20**, 74 (2024).
 - [55] K. W. Plumb, H. J. Changlani, A. Scheie, S. Zhang, J. W. Krizan, J. A. Rodriguez-Rivera, Y. Qiu, B. Winn, R. J. Cava, and C. L. Broholm, Continuum of quantum fluctuations in a three-dimensional $S = 1$ Heisenberg magnet, *Nature Physics* **15**, 54 (2019).
 - [56] R. Pohle and N. Shannon, Abundance of spin liquids in the $s=1$ bilinear-biquadratic model on the pyrochlore lattice, and its application to NaCaNi₂F₇, arXiv:2503.12776 (2025).
 - [57] A. J. Kim, N. V. Prokof'ev, B. V. Svistunov, and E. Kozik, Homotopic Action: A Pathway to Convergent Diagrammatic Theories, *Physical Review Letters* **126**, 257001 (2021).
 - [58] J. Feldmeier, W. Natori, M. Knap, and J. Knolle, Local probes for charge-neutral edge states in two-dimensional quantum magnets, *Physical Review B* **102**, 134423 (2020).
 - [59] E. J. König, M. T. Randeria, and B. Jäck, Tunneling Spectroscopy of Quantum Spin Liquids, *Physical Review Letters* **125**, 267206 (2020).
 - [60] E. J. Davis, B. Ye, F. Machado, S. A. Meynell, W. Wu, T. Mittiga, W. Schenken, M. Joos, B. Kobrin, Y. Lyu, Z. Wang, D. Bluvstein, S. Choi, C. Zu, A. C. B. Jayich, and N. Y. Yao, Probing many-body dynamics in a two-dimensional dipolar spin ensemble, *Nature Physics* **19**, 836 (2023).
 - [61] A. Hehn, N. Van Well, and M. Troyer, High-temperature series expansion for spin-1/2 Heisenberg models, *Computer Physics Communications* **212**, 180 (2017).
 - [62] D. A. S. Kaib, M. Möller, and R. Valenti, *Nonlinear Spectroscopy as a Magnon Breakdown Diagnosis and its Efficient Simulation* (2025), arXiv:2502.01746 [cond-mat].
 - [63] Y. Watanabe, S. Trebst, and C. Hickey, Exploring Two-dimensional Coherent Spectroscopy with Exact Diagonalization: Spinons and Confinement in 1D Quantum Magnets, *Physical Review B* **110**, 134443 (2024).
 - [64] G. Bornet, G. Emperauger, C. Chen, F. Machado, S. Chern, L. Leclerc, B. Gély, Y. T. Chew, D. Barredo, T. Lahaye, N. Y. Yao, and A. Browaeys, Enhancing a Many-Body Dipolar Rydberg Tweezer Array with Arbitrary Local Controls, *Physical Review Letters* **132**, 263601 (2024).
 - [65] B. Dalla Piazza, M. Mourigal, N. B. Christensen, G. J. Nilsson, P. Tregenna-Piggott, T. G. Perring, M. Enderle, D. F. McMorrow, D. A. Ivanov, and H. M. Rønnow, Fractional excitations in the square-lattice quantum antiferromagnet, *Nature Physics* **11**, 62 (2015).
 - [66] H. Shao, Y. Q. Qin, S. Capponi, S. Chesi, Z. Y. Meng, and A. W. Sandvik, Nearly Deconfined Spinon Excitations in the Square-Lattice Spin-1/2 Heisenberg Antiferromagnet, *Physical Review X* **7**, 041072 (2017).
 - [67] Y. Ran, M. Hermele, P. A. Lee, and X.-G. Wen, Projected-Wave-Function Study of the Spin-1/2 Heisenberg Model on the Kagomé Lattice, *Physical Review Letters* **98**, 117205 (2007).
 - [68] Y. Iqbal, F. Becca, S. Sorella, and D. Poilblanc, Gapless spin-liquid phase in the kagome spin-1/2 Heisenberg antiferromagnet, *Physical Review B* **87**, 060405 (2013).
 - [69] Y.-C. He, M. P. Zaletel, M. Oshikawa, and F. Pollmann, Signatures of Dirac Cones in a DMRG Study of the Kagome Heisenberg Model, *Physical Review X* **7**, 031020 (2017).
 - [70] S. Yan, D. A. Huse, and S. R. White, Spin Liquid Ground State of the $S=1/2$ Kagome Heisenberg Model, *Science* **332**, 1173 (2011).
 - [71] S. Depenbrock, I. P. McCulloch, and U. Schollwöck, Nature of the Spin-Liquid Ground State of the $S = 1/2$ Heisenberg Model on the Kagome Lattice, *Physical Review Letters* **109**, 067201 (2012).
 - [72] W. Zhu, X. Chen, Y.-C. He, and W. Witczak-Krempa, Entanglement signatures of emergent Dirac fermions: kagome spin liquid & quantum criticality, *Science Advances* **4**, eaat5535 (2018).
 - [73] O. Golinelli, T. Jolicoeur, and R. Lacaze, Finite-lattice extrapolations for a Haldane-gap antiferromagnet, *Physical Review B* **50**, 3037 (1994).
 - [74] S. R. White and I. Affleck, Spectral function for the $S = 1$ Heisenberg antiferromagnetic chain, *Physical Review B* **77**, 134437 (2008).

End Matter

Continued-fraction parameters: The parameters δ_r for $r = 4, 5, 6$ are given in terms of moments m_0, m_2, \dots, m_{2r} :

$$\delta_4 = \frac{m_2 (m_4^3 - (2m_2m_6 + m_0m_8)m_4 + m_0m_6^2 + m_2^2m_8)}{(m_2^2 - m_0m_4)(m_2m_6 - m_4^2)} \quad (12)$$

$$\delta_5 = -\frac{(m_2^2 - m_0m_4)(-m_6^3 + 2m_4m_8m_6 - m_2m_8^2 + (m_2m_6 - m_4^2)m_{10})}{(m_4^2 - m_2m_6)(m_4^3 - (2m_2m_6 + m_0m_8)m_4 + m_0m_6^2 + m_2^2m_8)} \quad (13)$$

$$\delta_6 = \frac{[(m_4^2 - m_2m_6)((3m_4m_8 + 2m_2m_{10} + m_0m_{12})m_6^2 - m_6^4 - 2((m_4^2 + m_0m_8)m_{10} + m_2(m_8^2 + m_4m_{12}))m_6) + m_0m_8^3 - m_4^2m_8^2 - m_2^2m_{10}^2 + m_0m_4m_{10}^2 + 2m_2m_4m_8m_{10} + (m_4^3 + (m_2^2 - m_0m_4)m_8)m_{12}]}{[(m_4^3 - (2m_2m_6 + m_0m_8)m_4 + m_0m_6^2 + m_2^2m_8)(m_6^3 - 2m_4m_8m_6 + m_2m_8^2 + (m_4^2 - m_2m_6)m_{10})]} \quad (14)$$

Moments and continued fraction parameters for the Heisenberg $S = 1/2$ AFM chain at $x > 0$: In Fig. 5 we provide details about the resummation of the Dyn-HTE moments $m_{\mathbf{k},2r}(x)$ for $x > 0$ and the parameters $\delta_{\mathbf{k},r}$ underlying the DSF in Fig. 2. We consider $\mathbf{k} = 0.2\pi$ and $\mathbf{k} = \pi$ in the left and right column, respectively. We find it convenient to show $x \cdot m_{\mathbf{k},2r}/m_{\mathbf{k},2r}(0)$ (top row), the factor x cancels the T which appears in the definition of the relaxation function and we thus expect a constant value for $x \rightarrow \infty$. The bare HTE series of $x \cdot m_{\mathbf{k},2r}/m_{\mathbf{k},2r}(0)$ is a polynomial of degree $n_{\max} - 2r + 1 = 13 - 2r$ and diverges around $x = 2$ (thin solid lines). Resummation uses Padé approximants after a change of variable $u = \tanh(fx)$, for the chain $f = 0.48$ shows good agreement between different Padé approximants. Due to the saturation of $\tanh(\cdot)$, x should not be larger than $O(2/f)$. In the bottom row we show the associated $\delta_{\mathbf{k},0}, \dots, \delta_{\mathbf{k},3}$ and the linear extrapolation for $\delta_{\mathbf{k},4}$ and higher (via a line through $\delta_{\mathbf{k},3}$ and the origin). Note that all $\delta_{\mathbf{k},r}$ are non-negative as required for a faithful $A_{\mathbf{k}}(\omega)$, but this might break for poor moment resummations.

Square-lattice Heisenberg $S = 1/2$ AFM: We apply Dyn-HTE to the nearest-neighbor model on the square-lattice which is unfrustrated and known to exhibit long-range Néel order in its ground state. At finite temperature, the spin correlation length becomes finite and the characteristic magnon excitations acquire a lifetime-broadening. The DSF of this model has been studied experimentally in a material realization [65] and numerically via quantum Monte Carlo [66]. In Fig. 6(left) we present the DSF from Dyn-HTE at $x = J/T = 2.0$ where the paramagnons emergent from low energy at $\mathbf{k} = (\pi, \pi)$ are already clearly discernible. The crosses denote the energy of the paramagnon mode as measured experimentally at $x \simeq 11$ [65]. Despite the difference in temperature, the agreement is reasonable. Another noteworthy feature of the Dyn-HTE data also observed in experiment is the suppression of the DSF at $(\pi, 0)$ as compared to $(\pi/2, \pi/2)$. However, at the temperatures accessible to Dyn-HTE, we fail too see the anomalous non-Gaussian DSF lineshape at $(\pi, 0)$ which was discussed as a possible signature of spinon deconfinement [65].

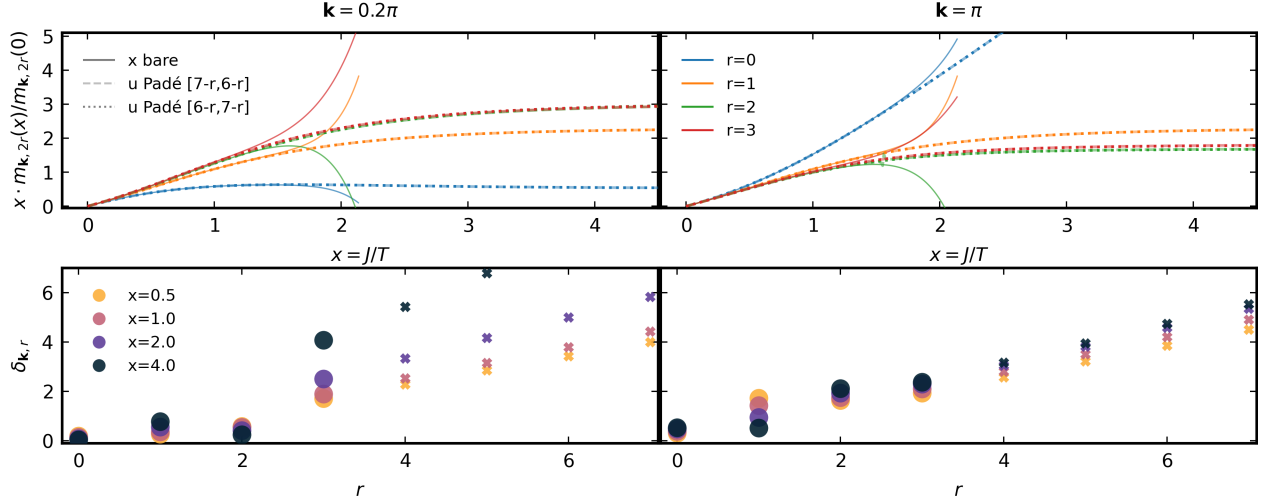


FIG. 5. Heisenberg $S = 1/2$ AFM chain: First four normalized moments $x \cdot m_{\mathbf{k},2r}(x)/m_{\mathbf{k},2r}(0)$, $r = 0, 1, 2, 3$ from Dyn-HTE (top) and corresponding continued fraction parameters $\delta_{\mathbf{k},r}$ (bottom) at momenta $\mathbf{k} = 0.2\pi$ (left) and $\mathbf{k} = \pi$ (right). The solid lines represent the bare series, while the dotted and dashed lines are different Padé approximants in the variable $u = \tanh(fx)$. We chose $f = 0.48$ such that the different Padé approximants agree with each other. The bottom row shows the corresponding δ_r of the continued fraction expansion at various temperatures (dots) and their linear extrapolation for $r \geq 4$ (crosses).

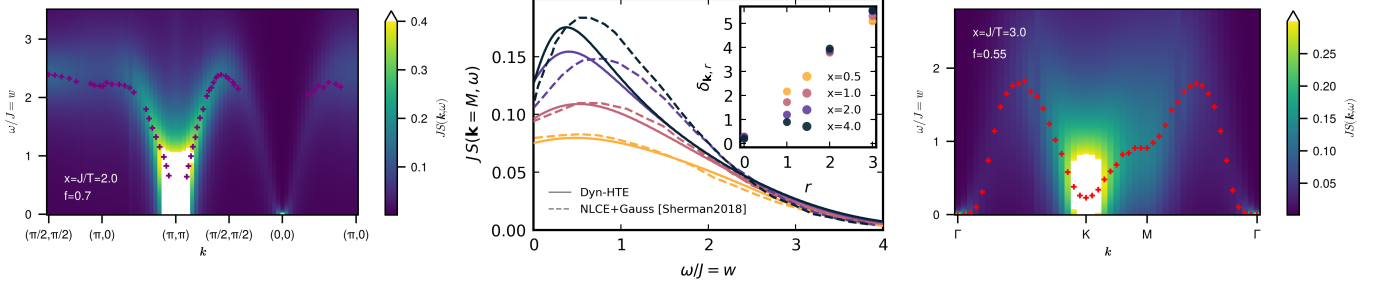


FIG. 6. DSF for $S = 1/2$ nearest-neighbor Heisenberg AFMs in 2D from Dyn-HTE calculated with $r_{max} = 3$. Left: Square lattice model at $x = J/T = 2$ ($f = 0.7$). Crosses denote the energy of the paramagnon mode measured experimentally at $x \simeq 11$ in Ref. [65]. Middle: Kagome lattice model, linecuts at momentum M in the extended Brillouin zone from Dyn-HTE with $r_{max} = 3$ and $f = 0.6$ (lines) and the NLCE results (dashed) from Ref. [26] which use only $r = 0, 1$ (Gaussian approximation). Inset: Continued fraction parameters δ_r for the four different temperatures $x = J/T$ from Dyn-HTE. Right: Triangular lattice model at $x = 3$ ($f = 0.55$). The red crosses denote the maximum obtained from the Dyn-HTE data at fixed momentum.

Kagome lattice Heisenberg $S = 1/2$ AFM: This frustrated nearest-neighbor model is defined by lattice vectors $\mathbf{e}_{1,2} = (1, \pm\sqrt{3})$ and a triatomic basis at the origin and at $(\pm 1, -\sqrt{3})/2$. The nature of the ground state remains under debate with certain evidence for either a gapless $U(1)$ Dirac QSL [67–69] or a gapped \mathbb{Z}_2 QSL [70, 71]. The DSF at $T = 0$ obtained from DMRG suffers from severe finite-size effects [72] especially at small $|\omega|$. For $x = J/T \leq 4$ the DSF has been calculated with NLCE [26] combined with the Gaussian approximation which constructs $A_{\mathbf{k}}(\omega)$ from moments $r = 0, 1$. Here we focus on the high-symmetry momentum $M = (0, 2\pi/\sqrt{3})$ and show the DSF from Dyn-HTE using four moments in Fig. 6(middle panel, full lines). Padé approximants of the u -series ($f = 0.6$) allow us to reach $x = 4$. For $x \leq 1$ the Dyn-HTE agrees well with NLCE results (dashed lines) but for larger x the line-shapes and peak-positions deviate significantly. In light of the close-to-linear $\delta_{\mathbf{k}, r}$ for the explicitly computed $r = 2, 3$ (inset) we are confident that the Dyn-HTE results with $\delta_{\mathbf{k}, r}$ extrapolation are quantitatively accurate for $x \leq 4$. At the K -point, the DSF (not shown) closely resembles a slightly scaled up version of the M -point data.

Triangular lattice Heisenberg $S = 1/2$ AFM: We supplement the linecuts shown in Fig. 3 with a plot of the DSF at $x = 3$ along a BZ path shown in Fig. 6(right panel). For each momentum, we denote the frequency with maximum DSF by a red cross. The shallow dip characterizing the roton-like excitation at $\mathbf{k} = M$ can already be inferred.

Heisenberg $S = 1$ AFM chain: As a benchmark for a $S = 1$ model we again consider the AFM Heisenberg chain which in contrast to its $S = 1/2$ counterpart features a gap of $0.41049(2)J$ [73]. In Fig. 7(a) we show the DSF obtained with Dyn-HTE at $x = 4$ for which the maximum of the dispersion agrees already closely to a ground state error-controlled tensor-network result [74] (red line). Note that the peak at $S(k = \pi, \omega)$ appears close to the Haldane gap. An important practical insight for the postprocessing of Dyn-HTE data can be gained from the attempt to compute the real-space on-site structure factor of the chain. From ground-state simulations [74] it is expected to feature a double-peak structure that will be softened by temperature. In principle, one could directly base its calculation on the Dyn-HTE series of the local Matsubara correlator, $G_{ii}(i\nu_m)$. However, it turns out that the result is much more robust and closer to the expected shape if one instead takes the \mathbf{k} -integral over the momentum resolved DSF of panel (a), this is shown in Figure. 7(b). The reason is that single-peak structures [as in $S(k, \omega)$] are more reliably obtained from a limited number of frequency moments $m_{\mathbf{k}, 2r}$ than more complicated lineshapes with multiple peaks.

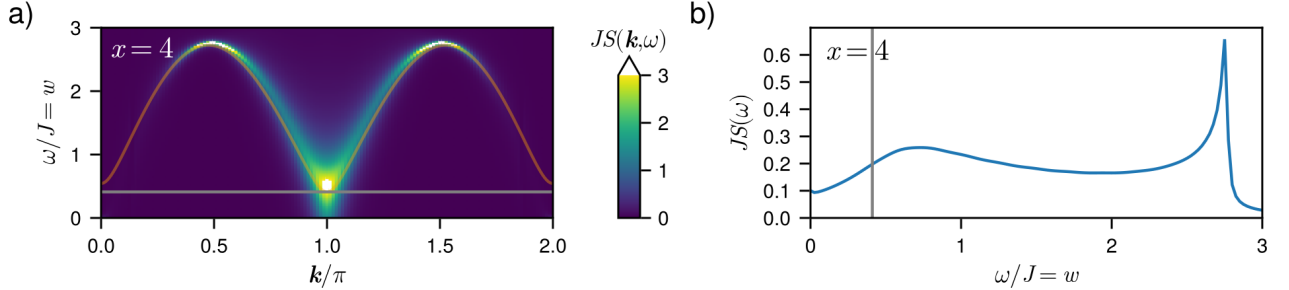


FIG. 7. $S = 1$ AFM Heisenberg chain. (a) DSF for $x = J/T = 4$ from Dyn-HTE with $r_{max} = 3$ and $f = 0.48$. The red line shows the maxima of the DSF at $T = 0$ obtained from DMRG [74]. (b) On-site DSF $S(\omega) = 1/(2\pi) \int_{-\pi}^{\pi} d\mathbf{k} S(\mathbf{k}, \omega)$ obtained from the data in panel (a). In both panels, the gray lines indicate the Haldane gap of $0.41049(2)J$ [73].